# Coexistence and coupling of zero-dimensional, two-dimensional, and continuum resonances in nanostructures

Voicu Popescu,[1] Gabriel Bester,[2] and Alex Zunger[1,*]
[1]*National Renewable Energy Laboratory, Golden, Colorado 80401, USA*
[2]*Max-Planck-Institut für Festkörperforschung, Heisenbergstraße 1, D-70569 Stuttgart, Germany*
(Received 30 April 2009; revised manuscript received 4 June 2009; published 31 July 2009)

Quantum dots (QDs) embedded in a matrix exhibit a coexistence of "zero-dimensional" (0D) bound electron and hole states on the dot with "three-dimensional" (3D) continuum states of the surrounding matrix. In epitaxial QDs one encounters also "two-dimensional" (2D) states of a quantum well-like supporting structure (wetting layer). This coexistence of 0D, 2D, and 3D states leads to interesting electronic consequences explored here using multiband atomistic pseudopotential calculations. We distinguish strained dots (InAs in GaAs) and strain-free dots (InAs in GaSb) finding crucial differences: in the former case "potential wings" appear in the electron confining potential in the vicinity of the dot. This results in the appearance of localized electronic states that lie *above the threshold* of the 3D continuum. Such resonances are "strain-induced localized states" (SILSs) appearing in strained systems, whereas in strain-free systems the dot resonances in the continuum are the usual "virtual bound states" (VBSs). The SILSs were found to occur regardless of the thickness of the wetting layer and even in interdiffused dots, provided that the interdiffusion length is small compared to the QD size. Thus, the SILSs are well isolated from the environment by the protective potential wings, whereas the VBSs are strongly interacting. These features are seen in our calculated intraband as well as interband absorption spectra. Furthermore, we show that the local barrier created around the dot by these potential wings suppresses the 0D-2D (dot-wetting layer) hybridization of the electron states. Consequently, in contrast to findings of simple model calculations of envelope function, 0D-to-2D "crossed transitions" (bound hole-to-wetting layer electron) are practically absent because of their spatially indirect character. On the other hand, since no such barrier exists in the hole confining potential, a strong 0D-2D hybridization is present for the hole states. We show this to be the source for the strong 2D-to-0D crossed transitions determined experimentally.

DOI: 10.1103/PhysRevB.80.045327 PACS number(s): 71.23.An, 73.21.La, 78.67.Hc

## I. INTRODUCTION

Of the many methods used to fabricate semiconductor quantum dots (QDs),[1–4] the Stranski-Krastanov epitaxial growth technique[4] has emerged as one producing some of the best QD materials in terms of structural perfection,[5,6] as evidenced, amongst others, by ultrasharp spectral lines.[7–9] The essential feature of this growth technique is that the QD (e.g., InAs) is embedded in a matrix made of a semiconductor material (e.g., GaAs) that must have a size mismatch with respect to the dot material. The process involves a morphological transition[4] from a two-dimensional (2D) to a zero-dimensional (0D) growth mode, so a 2D structure, called wetting layer (WL) is often present (Fig. 1).[3,4] Like a quantum well (QW), this 2D WL supports hole and electron bands, denoted in the following as $WL_h$ and $WL_e$. Such states coexist with the normal 0D bound electron and hole states of the QD. The existence of a 2D, in addition to the 0D, component is an important difference between epitaxial and colloidal QDs. In the present paper we analyze the *electronic* consequences of the coexistence of 0D states with 2D WL states and the corresponding 3D continuum states of the matrix.

This coexistence has a number of interesting consequences,[10] including lasing action of far infrared response,[11,12] nonlinear upconversion,[13] or dephasing of excited carriers.[14] Quasibound states in the continuum, so-called virtual bound states (VBSs), have long been known to occur in sharply varying (e.g., square well) potentials.[15,16] We will further see that the presence of strain between the QD and the matrix within which it is embedded creates a new kind of localized resonant states at energies within the 3D continuum, which we termed strain-induced localized states (SILSs).[17]

The electronic level diagram of a QD system can be thought of at first in a simple model [Fig. 2(a)], considering dot-localized 0D states, 2D WL states, 3D matrix states, and resonant VBS. Within such a setup, one would expect to observe the following transitions:

(i) dot-localized hole (electron) to dot-localized electron (hole) states [type 1 in Fig. 2(a)];

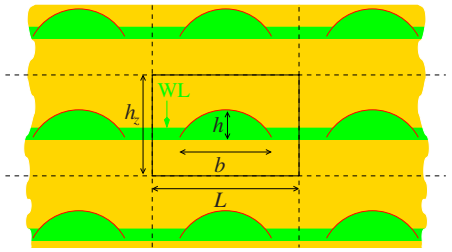


FIG. 1. (Color online) Schematic drawing of a self-assembled QD system including the QD of height $h$ and diameter $b$, a wetting layer (WL) of the same material and the matrix. Black solid rectangle marks the supercell of height $h_z$ and width $L$ used in the calculations.

 

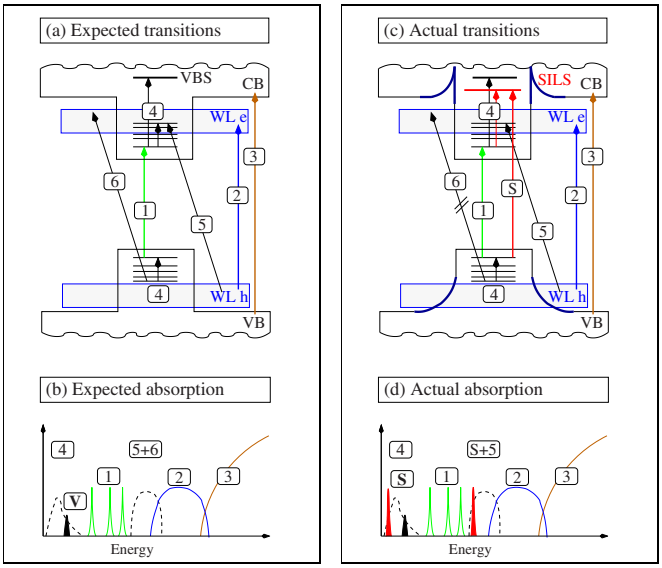


FIG. 2. (Color online) Schematic drawing of the expected and actually calculated transitions, and the corresponding spectra in QD systems.

(ii) 2D WL hole (electron) to 2D WL electron (hole) states [type 2 in Fig. 2(a)];

(iii) 3D matrix hole (electron) and 3D matrix electron (hole) states [type 3 in Fig. 2(a)];

(iv) dot-localized electron (hole) to 0D/2D/3D electron (hole) states [type 4 in Fig. 2(a)], which are intraband transitions, the basis for the proposed intermediate-band solar cells and infrared photodetectors based on quantum dots.[18–21] All these *direct* transitions are expected to show up as significantly strong peaks in the absorption spectrum, as schematically shown by the corresponding solid (colored) lines in Fig. 2(b).

In addition, Toda *et al.*[14] and Kammerer *et al.*[13,22] had observed pronounced peaks in the interband absorption, energetically located in the region between the transitions of types 1 and 2. Features as shown schematically in Fig. 2(b) by dashed lines and labeled as 5 and 6 were first assumed to originate from the WL. The existence of such "crossed transitions" between 2D-WL and 0D bound states was theoretically discussed by Vasanelli *et al.*[23] who suggested that these transitions could occur either between

(v) $WL_h$ and the dot-localized electron states [type 5 in Fig. 2(a)], denoted here as $WL_h \rightarrow e$, or between

(vi) dot-localized hole states and $WL_e$ [type 6 in Fig. 2(a)], denoted here as $h \rightarrow WL_e$.

We will focus on these two types of transitions, $h \rightarrow WL_e$ and $WL_h \rightarrow e$, in the present work. The starting point of our discussion is the current understanding, which can be summarized as follows: (a) $h \rightarrow WL_e$ transitions, type 6, were attributed experimentally[13,14,24] to carrier relaxation and photoluminescence upconversion; (b) $WL_h \rightarrow e$ transitions, type 5, were suggested as an explanation of the observed[25,26] pronounced peaks located between intradot and continuum transitions. Vasanelli *et al.*[23] determined fingerprints of transitions of types 5 and 6 within a single-band effective-mass approximation. They found that the $WL_h \rightarrow e$ transitions are stronger and energetically lower than $h \rightarrow WL_e$. Later experiments of Oulton *et al.*[25] and Mazur *et al.*[26] have used the model of Vasanelli *et al.*,[23] and found excellent agreement with its predictions for a $WL_h \rightarrow e$ crossed transition and their measured photoluminescence excitation data.

Significantly, the theoretical approach used previously[23] to describe the coupling between 0D and 2D states employed a particle-in-a-box model with a piecewise constant potential, neglecting the mutual deformation exerted by the respective strained potentials. We use here our atomistic multiband multivalley pseudopotential approach[27,28] to provide a comprehensive and realistic picture of the absorption processes in epitaxial QDs. We find that the coherent dot-matrix strain necessarily present in these systems distorts the confining potential,[29,30] a feature that has far-reaching consequences: (i) the electron confining potential (ECP) exhibits "wings" around the QD, which act as a local barrier, as depicted in Fig. 2(c); (ii) along the growth direction, the hole confining potential (HCP) becomes wider and smoother well above the matrix valence-band maximum. When such strained-induced distortions in the confining potential exist, the actual picture of the absorption spectra changes as schematically shown in Fig. 2(d):

(i) the wings in the ECP may lead to the appearance of SILS—red (gray) lines labeled accordingly in Fig. 2(c)—i.e., localized states *above* the continuum threshold,[17] which have very large oscillator strength in intraband absorption. We will show that the SILS are not affected by the presence of the WL and they can be seen also in the interband absorption.

(ii) The barrier formed by the wings repels continuum electron states from the immediate vicinity of the dot. As a result, the dipole matrix element for crossed transitions between such repelled continuum states and the dot-localized bound states is weaker by up to four-five orders of magnitude than the bound-to-bound one. We conclude that the $e \rightarrow WL_e$ (intraband) and $h \rightarrow WL_e$ (interband) transitions are strongly inhibited when strain is properly accounted for in the calculations.

(iii) The distortion of the HCP results in the appearance of a new type of dot-confined hole states. These states, existing even without a WL present in the structure, couple extremely efficient with the $WL_h$ states and are responsible for peaks attributed to $WL_h \rightarrow e$ transitions.

## II. COMPUTATIONAL METHOD

To isolate the effect of strain we consider a lens-shaped InAs dot in two matrices: (a) GaAs matrix, exerting compressive strain, and (b) GaSb matrix, having no strain with respect to InAs. For our calculations we construct a supercell with $\sim 2 \times 10^6$ atoms, shown schematically in Fig. 1, and consisting of the dot, the WL, and the matrix. The geometry of the InAs dot is defined by the diameter $b=25$ nm and the height $h=3.5$ nm. We consider InAs WL thicknesses of 0, 2, 4, and 6 monolayers (MLs). The presence of the substrate is accounted for by epitaxially matching the dot, the WL, and the matrix to the in-plane substrate lattice constant.

The strain is determined by allowing each atom in the supercell to relax independently so as to minimize the strain

energy obtained within a generalized[31] valence force field (VFF) functional.[32,33] The underlying electronic structure has been subsequently calculated using an atomistic pseudopotential approach.[27] Once a relaxed configuration is obtained, we place on each atom $\alpha$=In, Ga, As, and Sb a screened atomic pseudopotential that depends on the identity $\alpha$ of the atom and the local strain tensor $\underline{\varepsilon}$,[27]

$$v_\alpha(\vec{r},\underline{\varepsilon}) = v_\alpha(\vec{r},0)[1 + \gamma_\alpha \,\mathrm{Tr}(\underline{\varepsilon})], \tag{1}$$

with $\gamma_\alpha$ as a fitting parameter introducing a further dependence on the identity of the neighbors.[27] We used for the unstrained pseudopotentials $v_\alpha(\vec{r},0)$ the parameters given by Magri and Zunger,[34] determined by requiring that the bulk binaries described by $v_\alpha(\vec{r},0)$ fit target data, including experimental band energies at high-symmetry points and effective masses, local-density approximation (LDA) hydrostatic and biaxial deformation potentials as well as the unstrained LDA valence-band offsets between the various binary compounds.[35–37]

Given the pseudopotential of each atom $\alpha$ and the relaxed positions $\vec{R}_{n\alpha}$, we solve the single-particle Schrödinger equation

$$\left[-\frac{\beta}{2}\nabla^2 + \sum_{n,\alpha} \hat{v}_\alpha(\vec{r} - \vec{R}_{n\alpha}, \underline{\varepsilon}_n) + \hat{V}_{\mathrm{NL}}\right]\psi_i(\vec{r}) = E_i\psi_i(\vec{r}), \tag{2}$$

where $\hat{V}_{\mathrm{NL}}$ represents the nonlocal spin-orbit coupling potential and $\beta$, taken as 1.23, a scaling factor for the kinetic energy.[27] We use a basis set for $\psi_i(\vec{r})$ consisting of a strain-dependent linear combination of bulk bands[38] $u^{\lambda}_{\nu,\vec{k}}(\vec{r},\underline{\varepsilon})$, of band index $\nu$ and wave vector $\vec{k}$ of materials $\lambda \equiv$ InAs, GaSb, and GaAs.

We calculate, within a single-particle approximation, the interband and intraband absorption spectra $\mu_{he}(E)$ and $\mu_{ee}(E)$ given, respectively, by:[39]

$$\mu_{ee}(E) \propto \sum_{i>0} |M^{ee}_{0i}|^2 \delta(E^e_i - E^e_0 - E), \tag{3}$$

$$\mu_{he}(E) \propto \sum_{j\geq 0}\sum_{i\geq 0} |M^{he}_{ji}|^2 \delta(E^h_j - E^e_i - E), \tag{4}$$

with $E=\hbar\omega$ as the energy of the absorbed photon and $M_{ij}$ as the dipole matrix element between an initial hole/electron state $|\psi_i\rangle$ and a final electron state $|\psi_j\rangle$

$$M_{ij} = \langle\psi_j|\hat{\vec{r}}|\psi_i\rangle. \tag{5}$$

The corresponding absorption spectra will be compared for the systems with and without WL as well as considering strained InAs/GaAs and unstrained InAs/GaSb.

## III. STRAIN-MODIFIED CONFINING POTENTIALS: THE APPEARANCE OF STRAIN-INDUCED POTENTIAL WINGS

The existence of compressive strain between a *curve*-shaped dot and its matrix creates wings in the ECP.[29,40] These will be shown to have a major role in (i) creating strain-induced localized states above the continuum[17] and (ii) isolating the dot-confined states from the WL states, significantly weakening the dot-continuum hybridization.

We have calculated the confining potentials by means of an implementation of the Pikus-Bir model[41,42] but with the atomistic strain functional. The central quantities of this model are the unstrained band edge, its deformation potential $a$, and the local strain tensor $\underline{\varepsilon}(\vec{r})$. Thus, the strain-modified conduction-band minimum (CBM) $E_c$ is given by the formula

$$E_c(\vec{r}) = E^0_c + a_c \,\mathrm{Tr}[\underline{\varepsilon}(\vec{r})], \tag{6}$$

where $E^0_c$ is the unstrained CBM and $a_c$ is the conduction-band deformation potential. The valence-band edge dependence on the local strain takes on an equivalent, although more complicated form, as described in detail, for example, in Ref. 29. Equation (6) is evaluated using the local strain $\underline{\varepsilon}(\vec{r})$ as obtained by the VFF relaxation of the actual dot-WL-matrix system. The confining potentials $E_c(\vec{r})$ and $E_v(\vec{r})$ determined this way are not used in any further calculation and will be shown for illustration purposes only.

Corresponding strain-modified band offsets are presented in Fig. 3 for three systems: (a) the unstrained (lattice-matched) InAs/GaSb system without WL, (b) the strained (lattice-mismatched) InAs/GaAs system without WL, and (c) the InAs/GaAs system with a 4 ML thick WL. We see that no potential deformation occurs in the unstrained lattice-matched InAs/GaSb [panel (a)]; the total potential is piecewise constant, looking like a square well. In contrast, for strained InAs/GaAs [panels (b) and (c)], one notes the occurrence of wings in the ECP, outlined by thick black lines. These changes are the result of the interaction of the curved dot with the strain induced by the matrix. Indeed, if InAs and GaAs were forming flat interfaces (as is the case of a quantum well) then the biaxial strain would be constant and would not decay with position. However, if a curved object (e.g., lens-shaped QD) is inserted in an isotropic elastic matrix, the strain varies differently in the two regions:[43,44] whereas is linearly varying inside the QD, it decays rapidly inside the matrix, $\propto 1/r^3$, as the position varies from the dot proximity. This behavior leads to the distortion of the confining potentials in the vicinity of a spherical, pyramidal, or lens-shaped embedded dot. Such wings have been obtained for various strained systems, for both ECP and HCP,[29,40] results to which we refer the reader for a thorough quantitative discussion. Here we only emphasize on the *local* character of these distortions. Their formation and amplitude depend (through the lattice mismatch) on the strain induced near the dot, and on the band offsets between the dot and the matrix materials. In contrast, they are independent on the vertical and/or lateral dot-dot separation as well as on the size of the supercell used in the simulation. By comparing panels (b) and (c) of Fig. 3, we further see that the WL *does not* qualitatively modify the confining potential in the vicinity of the dot. This result will turn to be of particular importance in further discussion on transitions previously associated with a WL (i.e., $\mathrm{WL}_h \rightarrow e$), which we found to exist even *without* a WL included in the structure.

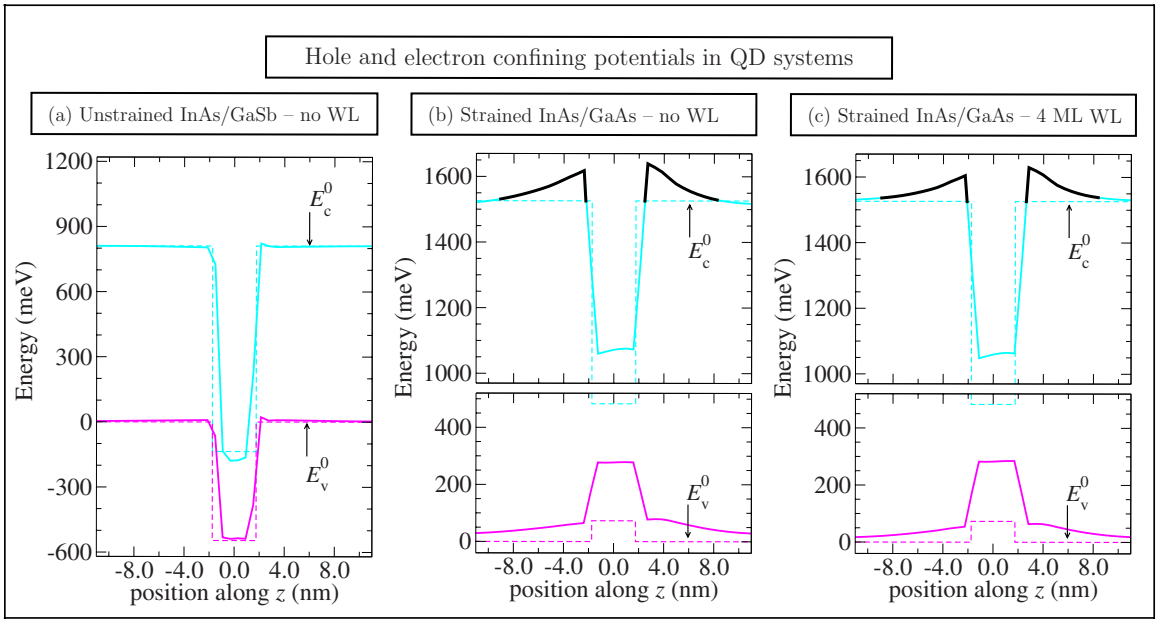


FIG. 3. (Color online) Line plots of the hole (magenta/grey) and electron (cyan/light grey) strain-modified confining potentials for various QD systems: (a) unstrained InAs/GaSb without WL; (b) strained InAs/GaAs without WL; (c) strained InAs/GaAs with a 4 ML thick WL. The unstrained band edges of the corresponding matrix and dot materials are shown with dashed lines, and labeled as $E_c^0$ and $E_v^0$, respectively. For all the plots, the confining potentials are shown along a line going through the dot center parallel to the $z$ axis. Energy zero is the VBM of each of the matrices.

## IV. SURVEY OF EIGENSTATES IN QD SYSTEMS

### A. Prototype states and their wave functions

The different eigenfunctions of the single-particle problem [Eq. (2)] can be classified according to:[17] (a) their degree of localization ("$L$") or delocalization ("$D$") in vertical [001] ($z$) and lateral ($xy$) directions, and (b) the probability $p_{dot}^i$ to find the particle in state $i$ inside the dot volume $\Omega_{dot}$

$$p_{dot}^i = \int_{\Omega_{dot}} d^3r |\psi_i|^2. \tag{7}$$

Figure 4 shows prototype *electron* wave functions for each of these types. We note that this classification is applicable also for hole states (not shown). One finds:

(i) *dot-localized bound states* [Fig. 4(a)] with wave functions of type $L_zL_{xy}$ and significant $p_{dot}$ values ($\geq$0.50);

(ii) *unbound states*, type $D_zD_{xy}$ [Fig. 4(b)], delocalized both vertically and laterally, with rather small $p_{dot}$ values, not exceeding 0.02;

(iii) *vertically localized and horizontally delocalized states*, type $L_zD_{xy}$, associated with the 2D structure, Fig. 4(c).

(iv) *Hole* $D_zL_{xy}$ *states*, i.e., hole states delocalized in the $z$ direction but dot-confined in the $xy$ plane, with typical $p_{dot}$ values in the range of 0.20–0.50. Representative wavefunction plots for these states are shown in Fig. 5. Their existence is a consequence of the strain-induced distortion of the HCP. As it is obvious from Fig. 3(b), the potential well for holes "opens" about 100 meV above the matrix valence-band maximum (VBM) $E_v^{\text{mat}}$ in the $z$ direction, whereas is still "closed" (not shown) in the $xy$ plane. This creates a smooth transition between the $L_zL_{xy}$ and $D_zD_{xy}$ hole states over the energy interval of $E_v^{\text{mat}} \cdots E_v^{\text{mat}} + 100$ meV. As we will show below, the hole-$D_zL_{xy}$ states play a central role in the $\text{WL}_h \rightarrow e$ crossed transitions.

(v) *VBS* (Fig. 6), characterized by a certain space localization inside the dot (large $p_{dot}$) and energetically located within the continuum of the 2D/3D states. Such states are known to emerge from the one-dimensional motion of a particle in a potential well of depth $-V$. For the *unbound* motion, when $\varepsilon > 0$, the constructive interference inside the slab leads to the appearance of VBS, which occur at discrete energies, similar to the confined bound states, but, unlike those, are characterized by a finite lifetime. Whereas analytical models for the potential allow one to evaluate the VBS eigenvalues, their broadening, and lifetime,[10,45] our numerical determination is inherently sensitive to the size of both supercell and the basis set used in the calculations. We obtain a dense ladder of states describing the barrier continuum with an average spacing of $\simeq$1 meV. The VBSs are broadened due to the interaction with the continuum, the broadening being reflected in Fig. 6 by the two eigenstates, separated by only 0.4 meV, which belong to the same VBS.

(vi) *SILS*,[17] which are localized states *above* the matrix CBM and below the potential wings, appearing as a direct consequence of the local barrier created around the QD by the wings in the ECP discussed above. The SILS can be either of type $L_zD_{xy}$, i.e., somewhat delocalized horizontally,[17] or of type $L_zL_{xy}$, as shown in Fig. 7. We note here that the localization of these states follows the strain-modified confining potential [Figs. 3(b) and 3(c)], not the strain itself. Being above the CBM, the $L_zL_{xy}$ SILSs are therefore tunnel coupled to the continuum states of the barrier. In contrast to the VBS, however, which interact directly with the continuum, the SILSs are efficiently shielded from

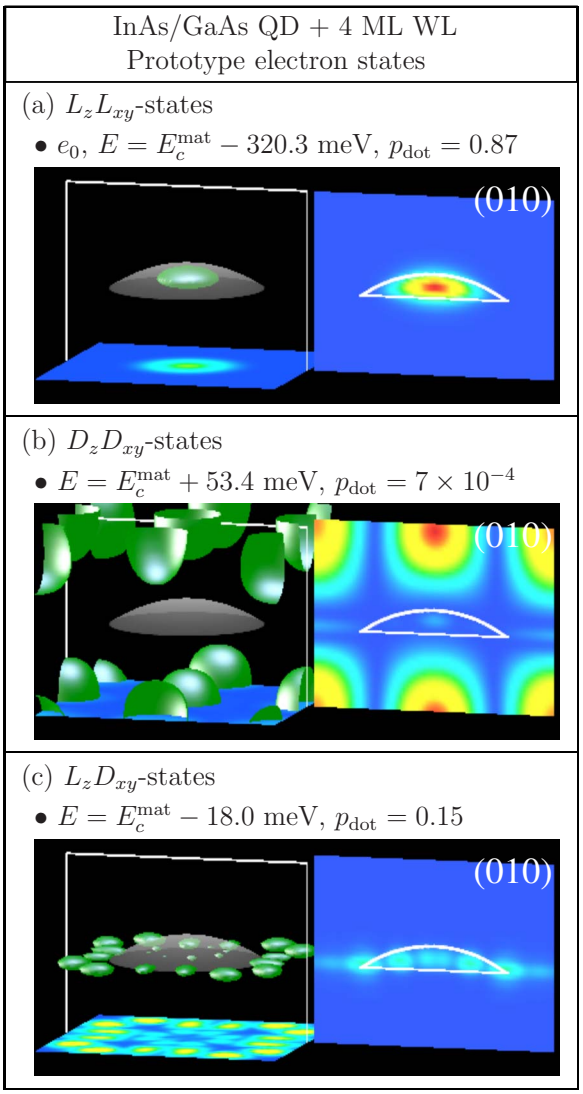


FIG. 4. (Color online) Wave-function plots of prototype electron states calculated for the InAs/GaAs dot on GaAs(001) substrate, with a 4 ML thick WL. The energies of the states are given with respect to GaAs CBM $E_c^{\mathrm{mat}}$ while $p_{dot}$ is the amount of $|\psi|^2$ comprised inside the dot. Isosurfaces (left side of each panel) are of constant value 0.4. Cross-section contour plots are shown on a blue-to-red (black-to-gray for 0.0–1.0) color scale. The crossing planes (moved from their original positions) go through the middle of the dot (shape shown in grey) and have (001) and (010) orientations.

the continuum by the potential wings and exist as sharp levels within an energetic resolution of $\simeq 1$ meV.

### B. Stability of strain-induced localized states against interfacial interdiffusion and wetting layer thickness

The occurrence of SILS is influenced by the dot geometry and the amplitude of the wings. Thus, in a taller dot, an $L_zL_{xy}$ SILS becomes a true dot-confined state, whereas it turns into a conventional VBS for flatter dots. The amplitude of the potential wings, on the other hand, depends on the QD/matrix lattice mismatch and band offsets. Hence, alloying of either the QD or matrix material may lead to the disappearance of SILS, as we could observe for $In_{0.4}Ga_{0.6}As$ in GaAs QD.[17] In the following we analyze the question of how robust the SILSs are with respect to the presence of a WL and In-Ga interdiffusion at the QD/matrix interface.

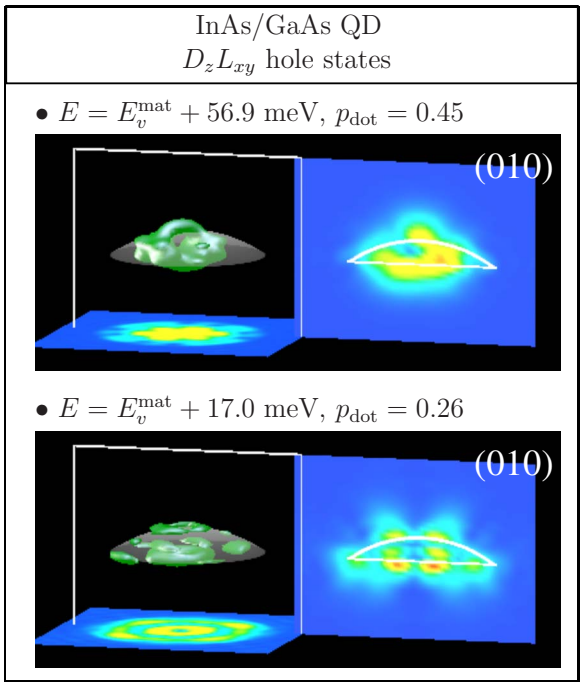


FIG. 5. (Color online) Wave-function plots of $D_zL_{xy}$-type hole states calculated for the InAs/GaAs dot on GaAs(001) substrate, without WL. The energies of the states are given with respect to GaAs VBM $E_v^{\mathrm{mat}}$ while $p_{dot}$ is the amount of $|\psi|^2$ comprised inside the dot. The layout of the plots is the same as in Fig. 4.

#### 1. Effect of wetting layer on SILS

The efficient shielding provided by the wings is illustrated in Fig. 7 by comparing the same SILS in the system without WL [Fig. 7(a)] versus the system with a 4 ML WL [Fig. 7(b)]. We have determined the 2D continuum onset of this system to be at 120 meV below the GaAs CBM. We see no significant qualitative changes in the SILS appearance. Although its position relative to GaAs CBM is 13 meV lower in the system with WL [Fig. 7(b)] as compared to the system without [Fig. 7(a)], the SILS is practically isolated from the 2D continuum, despite being well above its onset.

#### 2. Effect of interfacial interdiffusion on SILS

Interdiffusion can occur at the interface between InAs dot and the GaAs matrix as a result of capping of the dot by GaAs and/or postgrowth annealing. This is known to influence to a large extent the optical properties of InAs/GaAs QDs, both in intraband[46] and interband[47] transitions, causing a blueshift in the photoluminescence and a decrease in the sublevel spacing. Thorough theoretical investigations dealt with these effects in the past, e.g., Ref. 48, but not for SILS.

We describe the In/Ga composition profile following a Fickian model.[49,50] Starting from a steplike distribution $u_0(r)$, the interdiffused distribution $u(r)$ is obtained from the equation

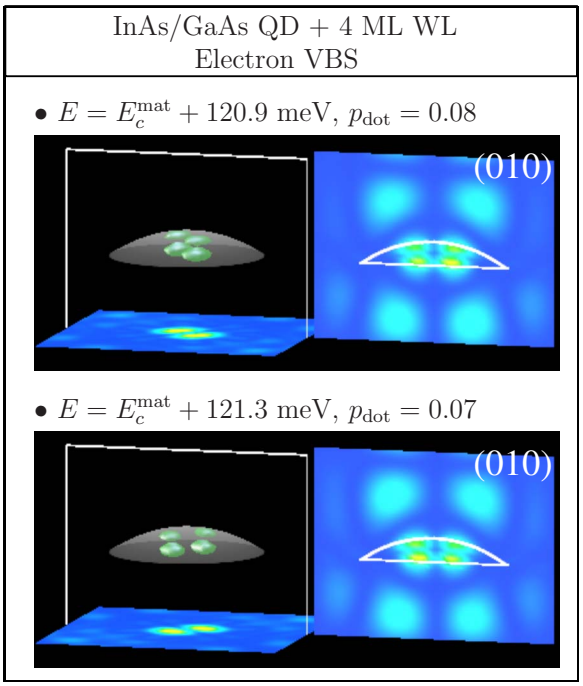


FIG. 6. (Color online) Wave-function plots of two eigenstates belonging to the same VBS, calculated for the InAs/GaAs dot on GaAs(001) substrate, with a 4 ML thick WL. The energies of the states are given with respect to GaAs CBM $E_c^{\mathrm{mat}}$ while $p_{dot}$ is the amount of $|\psi|^2$ comprised inside the dot. The layout of the plots is the same as in Fig. 4.

$$u(r) = \frac{1}{2\sqrt{\pi}L_D}\int \frac{u_0(r)}{r}\left\{\exp\left[\frac{(r-R)^2}{4Dt}\right] - \exp\left[\frac{(r+R)^2}{4Dt}\right]\right\}RdR, \tag{8}$$

where the diffusion length $L_D$ depends on the diffusion coefficient $D$ as $L_D = \sqrt{Dt}$ and is the only parameter entering Eq. (8). This simple model does not properly distinguish between Ga diffusing into InAs or In diffusing into GaAs, nor does it represent the dependence of diffusion on individual (Ga or In) activation barriers, or on growth temperature. More realistic interdiffusion profiles, which take into account these facts, can be calculated based on a kinetic model for molecular beam epitaxy growth, as developed, for example, for InAs/GaSb.[34] Nevertheless, the simple Fick model of Eq. (8) is qualitatively suited for our present purpose to investigate whether interfacial interdiffusion destroys the SILS.

We find that SILSs are still present when interdiffusion is accounted for, provided that the diffusion length $L_D$ is small compared to the size of the dot. In modeling our systems, we have started from a reference InAs/GaAs QD with abrupt interface $u_0(r)$, height $h=3.5$ nm, diameter $b=25$ nm, and a 2 ML thick WL, for which SILSs were found to exist. We considered two situations, of a small and a large interdiffusion, taking $L_D=0.56$ nm and $L_D=2.24$ nm, respectively, in Eq. (8). Since the variable $r$ in this equation is not continuous, the interdiffusion profiles were determined monolayer-wise (each ML of thickness $\simeq 0.28$ nm).

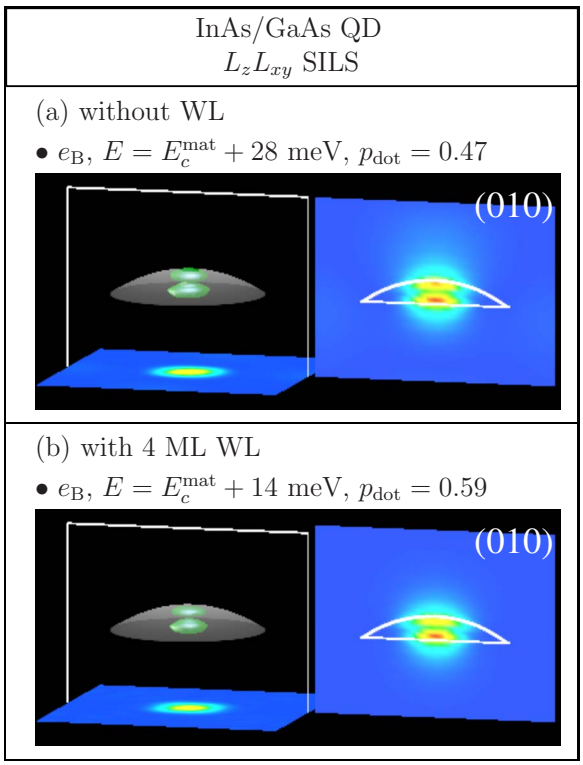


FIG. 7. (Color online) Wave-function plots of a SILS of type $L_zL_{xy}$ calculated for the InAs/GaAs dot on GaAs(001) substrate, (a) without a WL as compared to (b) including a 4 ML thick WL. The energies of the states are given with respect to GaAs CBM $E_c^{\mathrm{mat}}$ while $p_{dot}$ is the amount of $|\psi|^2$ comprised inside the dot. The layout of the plots is the same as in Fig. 4.

The resulting interdiffusion profiles for In (green/light gray) and Ga (red/dark gray) are shown in Fig. 8 for the three systems: (a) the reference QD with abrupt interface $u_0(r)$, (b) the slightly interdiffused ($L_D=0.56$ nm) QD, and (c) the strongly interdiffused ($L_D=2.24$ nm) QD. For QD (b), Eq. (8) gave a profile that equally intermixed In and Ga inside the QD on a length of $L_D=0.56$ nm out of its total height of 3.5 nm. In the case of QD (c), with $L_D=2.24$ nm, interdiffusion inside the dot occurs on a length of $\sim 1.68$ nm (corresponding to 3 ML). We allowed interdiffusion only on the convex QD/matrix interface but not within the WL, which acts as a buffer. After each random realization of an interdiffused interface, the atomic positions were relaxed so as to minimize the VFF elastic energy and then the single-particle problem was resolved.

The main effects of interdiffusion on SILS are summarized in Fig. 9. In this figure, we show the ECP and the energetic positions of the first electron-confined state $e_0$ and of the SILS $e_{\mathrm{B}}$. By allowing interdiffusion, we observe two trends in the ECP: (i) the wings become smoother and of lower amplitude; this effect is negligible for small $L_D$, system QD (b), but pronounced for big $L_D$. (ii) the width of the effective confinement becomes narrower as $L_D$ increases.

As a result, starting from the reference system with abrupt InAs/GaAs interface QD (a), characterized by $E(e_0)=1220$ meV and $E(e_{\mathrm{B}})=1556$ meV, a blueshift of the first-confined level occurs, in line with previous theoretical

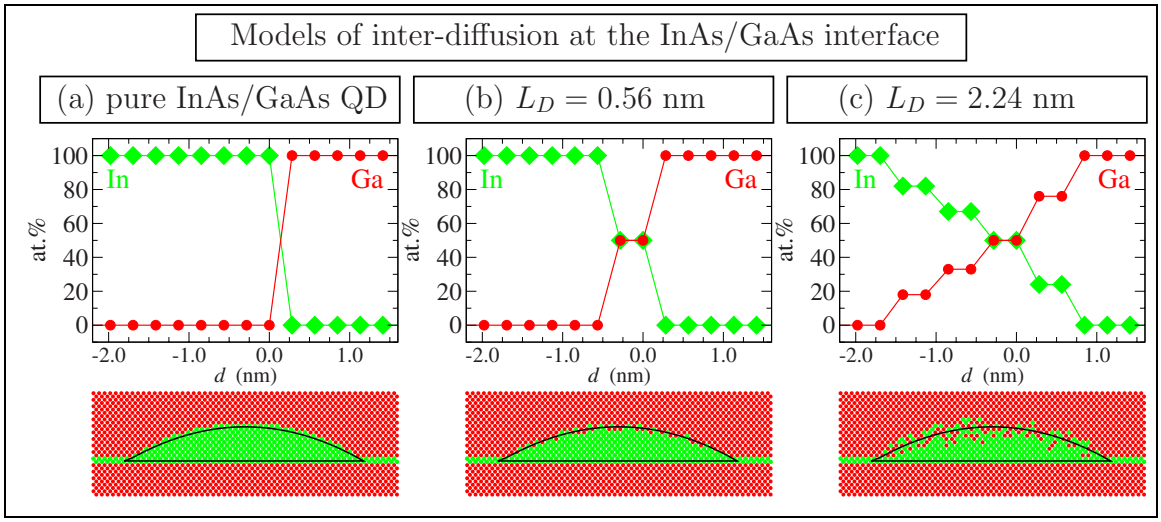


FIG. 8. (Color online) Interdiffusion profiles (top) and corresponding cross-sections (bottom) for the three InAs/GaAs QD systems used to investigate the effect of interface interdiffusion on SILS. The origin of the abscissa corresponds to the InAs/GaAs interface. (a) The reference QD, without interdiffusion, of diameter $b$=25 nm and height $h$=3.5 nm, with a WL thickness of 2 ML; (b) the QD from (a) accounting for an interdiffusion with depth $L_D$=0.56 nm; and (c) The QD from (a) accounting for an interdiffusion with depth $L_D$ =2.24 nm. Green (light gray) and red (dark gray) bullets depict the In and Ga atoms, respectively. Black solid contour shows the boundary of the reference QD (a).

results.[48,49] This blueshift is 14 meV for QD (b) ($L_D$ =0.56 nm) and 74 meV for QD (c) ($L_D$=2.24 nm). We could find the SILS level $e_B$ in the slightly interdiffused system QD (b), blueshifted by $\simeq$25 meV with respect to the reference system QD (a). As $L_D$ increases, system QD (c), the wings are less pronounced and the confinement region is smaller, the SILS $e_B$ is no longer present. However, we could identify for QD (c), at 140 meV above the GaAs CBM, a VBS of the typical width of $\simeq$1 meV, with the same appearance as the $e_B$ SILS. Thus, in a similar manner as for (In,Ga)As/GaAs QDs,[17] SILSs appear to morph into VBSs when the strain-induced local barrier becomes weaker. We conclude that, while the QD/matrix interdiffusion certainly modifies quantitatively the electronic structure of the QD, the SILSs appear to be relatively robust, provided that the interdiffusion length is small as compared to the height of the QD.

Based on these results, our further calculations rely on the simpler construction of a sharp interface QD/matrix. We will show that: (i) in the intraband absorption SILSs exhibit similar appearance, regardless on whether the WL is included or not in the calculation;[17] (ii) neither SILS nor VBS appear to interact with the 2D WL continuum when the ECP is distorted by strain; (iii) transitions with SILS as final states can be observed also in the intraband absorption as sharp well-defined peaks.

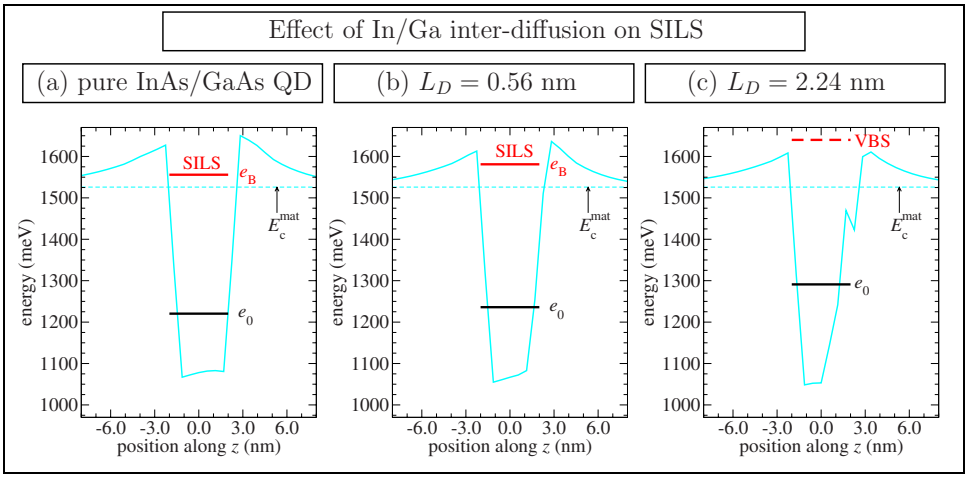


FIG. 9. (Color online) Line plots of the strain-modified electron confining potentials (cyan/light grey) for the three QD systems modeled in Fig. 8. Also shown, by horizontal lines, are the energy levels of the first-confined electron state $e_0$ and of the SILS state $e_B$, where this was found. Energy zero is the GaAs VBM.

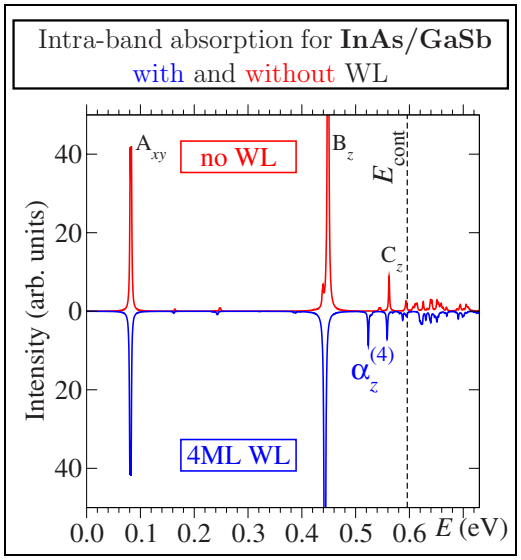


FIG. 10. (Color online) Intraband absorption spectra for the InAs/GaSb QD system: with (blue/bottom) and without (red/top) a WL included in the structure. The spectra were broadened using a Lorentzian of 1 meV FWHM. The vertical dashed line marks the continuum onset $E_{\text{cont}}=E_c^{\text{mat}}-E(e_0)$.

## V. CROSSED TRANSITIONS IN INTRABAND ABSORPTION

We have calculated the intraband absorption spectra for the two QD systems: the unstrained InAs/GaSb and the strained InAs/GaAs. For these systems, with confining potentials illustrated in Fig. 3, we consider both situations, with and without a WL in the structure. Initial state for all of the intraband spectra shown here is the first (S-like) electron confined level $e_0$. Correspondingly, the intraband absorption spectrum is calculated using Eq. (3), with the delta function replaced by a Lorentzian of full width at half maximum (FWHM) of 1 meV.

### A. Unstrained InAs/GaSb system: $e \rightarrow \text{WL}_e$ transitions are possible

Intraband absorption spectra for the InAs/GaSb QD are shown in Fig. 10, comparing the system without WL (top) against the one with a 4 ML thick WL included in the structure (bottom). In the unstrained InAs/GaSb system the absence of strain leads to a flat steplike confining potential, as can be seen in Fig. 3(a). We will show in the following that, in this case, the inclusion of the WL in the structure leads to a hybridization of high energy dot-confined states ($e$) with the WL states ($\text{WL}_e$). As a result, the absorption spectrum is affected by the presence of the WL.

Below the continuum onset $E_{\text{cont}}=E_c^{\text{mat}}-E(e_0)$, marked in Fig. 10 by a vertical dashed line, we observe the transitions $\text{A}_{xy}$, $\text{B}_z$, and $\text{C}_z$ (subscript indicates the light polarization) that are all $e \rightarrow e$ type ($L_zL_{xy} \rightarrow L_zL_{xy}$ or S $\rightarrow$ P like) and hence direct. They are present for *all* systems, with or without WL, and the variations in their energetic positions are very small (within 4–5 meV) when the thickness of the WL is changed. We show in Fig. 11(a) the final state $e_{\text{C}}$ of transition $\text{C}_z$.

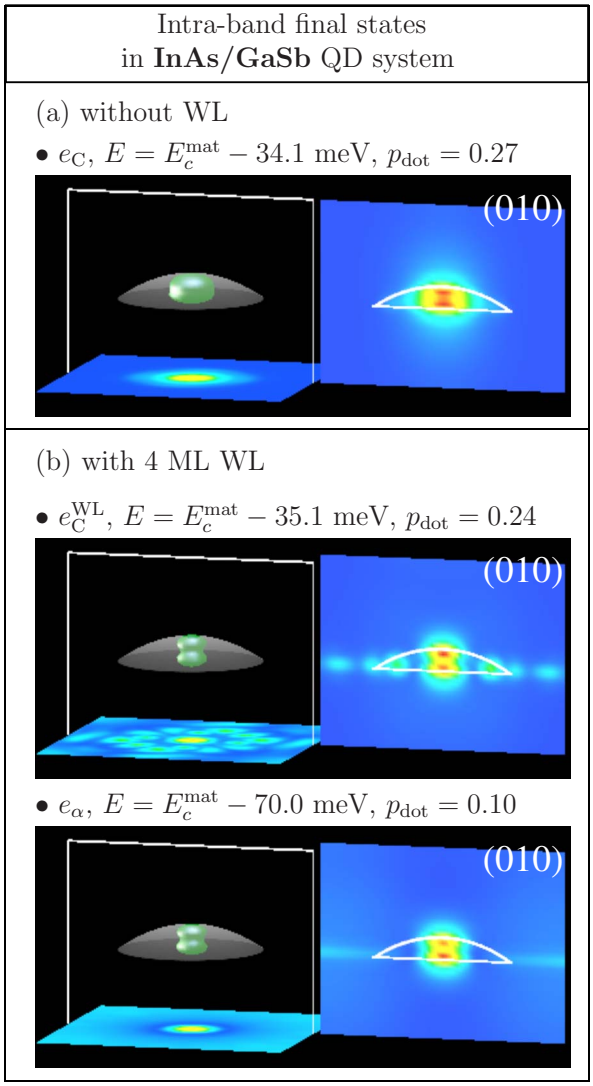


FIG. 11. (Color online) Wave-function plots of the final states $e_{\text{C}}$ and $e_\alpha$ of the intraband absorption spectra in Fig. 10. The energies of the states are given with respect to GaSb CBM $E_c^{\text{mat}}$ while $p_{dot}$ is the amount of $|\psi|^2$ comprised inside the dot. Layout of the plots follows the pattern of Fig. 4.

When a 4 ML thick WL is included in the structure, a strong transition, labeled in Fig. 10 as $\alpha_z^{(4)}$ (superscript indicating WL thickness), appears close to the slightly shifted $\text{C}_z$ peak. As can be seen in Fig. 11(b), the corresponding $e_\alpha$ final state is a *hybrid* $e$-$\text{WL}_e$ state, taking on the shape of the dot-confined $e_{\text{C}}$ state. We also note the behavior of the energetically higher-lying dot state $e_{\text{C}}$: whereas the peaks corresponding to $e_{\text{A}}$ and $e_{\text{B}}$ do not change with the inclusion of the WL, the $\text{C}_z$ peak, located within the $\text{WL}_e$ continuum, becomes of lower intensity. This is yet a further indication of an $e$-$\text{WL}_e$ hybridization.

Figure 12 shows the intraband absorption in InAs/GaSb for various thicknesses of the WL. We note that no $\alpha$ transition occurs for a thickness of 2 ML. For a 6 ML WL, in turn, the number of $\alpha$ peaks increases, and the influence of the 2D continuum on the dot-confined $e_{\text{C}}$ state, which shifts higher in energy, is even stronger.

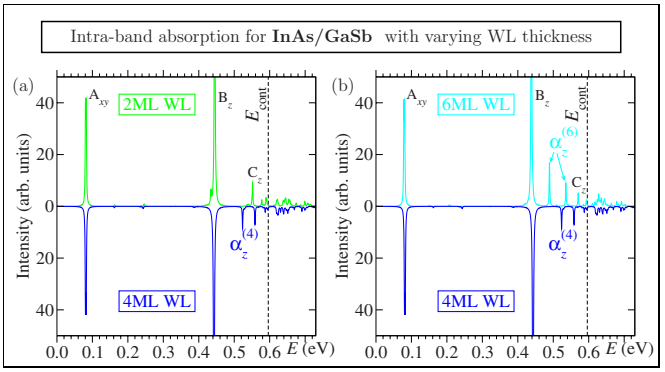


FIG. 12. (Color online) Intraband absorption spectra for InAs/GaSb QD system with a WL of varying thickness included in the structure. Comparison is made between the systems with: (a) 2 ML versus 4 ML and (b) 6 ML versus 4 ML thickness. The spectra were broadened using a Lorentzian of 1 meV FWHM.

These features can be understood in terms of the hybridization model depicted in Fig. 13. Although one can only approximately disentangle the QD effects from those of the superlattice,[10] such a model is expected to give a fairly good prediction on the evolution of states in the full system. Let us consider an InAs/GaSb quantum well (QW) with the InAs QW thickness $m$ ML, and having a state $E_c^{(m)}(2D)$ of symmetry compatible with the QD state $e_C$. The energetic position of $E_c^{(m)}(2D)$ will depend on $m$ in a similar monotonic manner as shown, for example, by Piquini *et al.*[51] for the CBM. When forming the whole system (matrix+WL+QD), the two states $E_c^{(m)}(2D)$ and $e_C$ will hybridize, giving rise to bonding-antibonding states as those shown in the middle of Fig. 13.

For this rather unusual case of no-strain InAs/GaSb system, the actual calculated intraband absorption spectra basically follow the expectations of the model and of the simple diagram depicted in Fig. 2(a). Similar theoretical results were obtained in the past using an effective-mass description[12,23,52] for *strained* systems. Because of neglecting the strain-induced changes in the confining potential, these results are not generally valid, as it will be shown in the following.

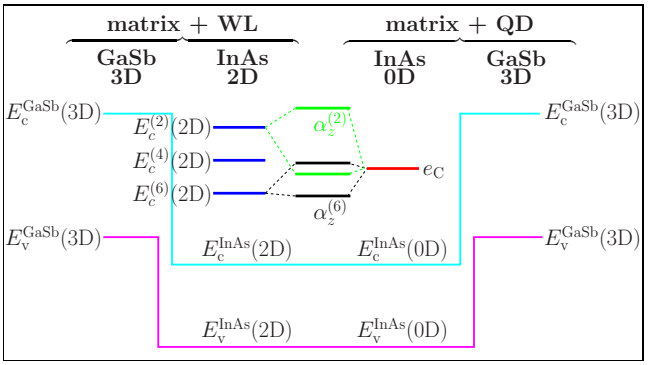


FIG. 13. (Color online) Quantum dot wetting layer hybridization model for the unstrained lattice-matched InAs/GaSb system.

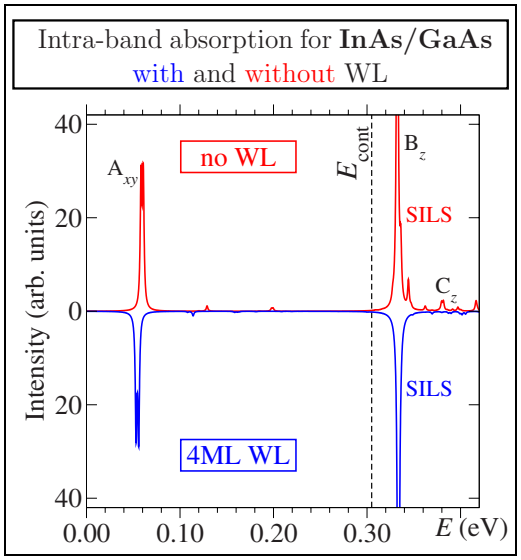


FIG. 14. (Color online) Same as Fig. 10 but for the InAs/GaAs QD system.

### B. Strained InAs/GaAs system: $e \rightarrow WL_e$ transitions are blocked

The intraband absorption spectrum for the InAs/GaAs QD system is shown in Fig. 14. We see, below the continuum onset $E_{cont}$, only S→P-like transitions ($e_0 \rightarrow e_{1,2}$). Similar to the case of no-strain InAs/GaSb, these are barely affected by the inclusion of the WL. *In contrast* to InAs/GaSb, there are *no WL-related* transitions appearing below continuum, for any of the investigated WL thicknesses (2, 4, and 6 MLs). This indicates that, unlike the unstrained system, here, for InAs/GaAs, there is only a weak hybridization between dot $e$ and $WL_e$ states. Thus, the predictions arising from the hybridization model (discussed above for InAs/GaSb) do not hold for real, strained systems.

The final state of transitions labeled by $B_z$ ($e_B$) in Fig. 14 is the SILS shown in Fig. 7. As pointed out above, its energetic location and appearance are not affected much by the presence of the WL. Unlike the $e_C$ state of strain-free InAs/GaSb, the SILS of InAs/GaAs shows practically no hybridization with the $WL_e$ continuum because of the "shield" provided by the potential wings, despite its position within the $WL_e$ band.

Figure 14 shows that, for the InAs/GaAs system, the number of peaks (strong transitions) above continuum is much reduced as compared to InAs/GaSb. The origin of these peaks, e.g., $C_z$ in top panel of Fig. 14, are, like in InAs/GaSb, the VBS. We note here the disappearance of the $C_z$ peak for the system with WL included (bottom panel of Fig. 14). This is the direct result of a change in the VBS resonance condition (a different structure) and not of a QD-WL hybridization. We therefore conclude that *the potential wings act as effective shields for both* $L_zL_{xy}$ and VBS states in preventing the hybridization with the $WL_e$ states. We will show below that, for a similar reason, crossed transitions of the type (hole-$L_zL_{xy}$)→$WL_e$ are likewise efficiently blocked, i.e., very weak.

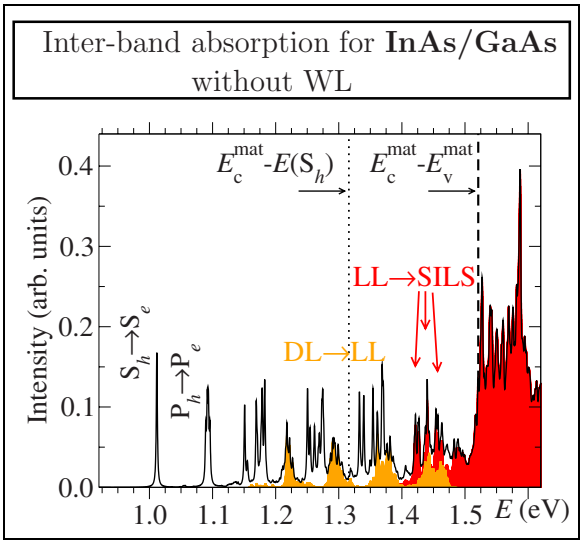


FIG. 15. (Color online) Interband absorption spectrum for InAs/GaAs QD system, without a WL included in the structure. Spectrum has been broadened using a Lorentzian of 1 meV FWHM. Areas highlighted in red (dark grey) show all hole→unbound-electron transitions, whereas transitions of the type hole-$D_zL_{xy}$ →electron-$L_zL_{xy}$ are shown in orange (light grey).

## VI. CROSSED TRANSITIONS IN INTERBAND ABSORPTION

The calculated interband absorption spectra for the InAs/GaAs QD system, (a) without and (b) with a WL included in the structure are shown in Figs. 15 and 16, respectively. Analogously to the intraband absorption, the calculations were performed using the single-particle approximation, Eq. (4), with the delta function replaced by a Lorentzian of FWHM of 1 meV. In both figures, the continuum threshold, corresponding to the GaAs band gap $E_{\rm gap}=E_c^{\rm mat}-E_v^{\rm mat}=1.521$ eV, is marked by a vertical thick-dashed line. We will therefore find bound-to-bound ($L_zL_{xy}\rightarrow L_zL_{xy}$ or $h\rightarrow e$) transitions only left of the $E_c^{\rm mat}-E_v^{\rm mat}$ line. The first of those transitions can be seen as sharp peaks in Figs. 15 and 16, and are labeled by capital letters (S and P) corresponding to the orbital character of the bound states. Our calculations for intraband absorption presented in Sec. V revealed that the electron 2D/3D continuum states manifest differently, depending on the strain present in the structure. The most significant result we obtained was that a simple energy diagram, with a steplike confining potential only applies to unstrained systems. However, previous theoretical interband absorption investigations[23] relied on such a model, which is inappropriate for strained systems, e.g., InAs/GaAs.

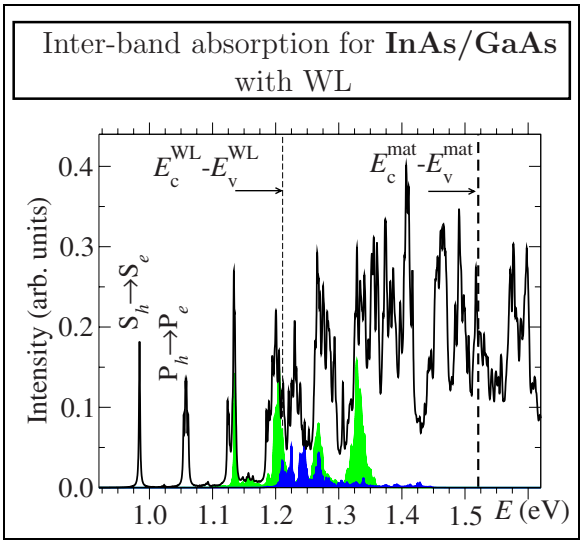


FIG. 16. (Color online) Interband absorption spectrum for InAs/GaAs QD system, with a 4 ML WL included in the structure. Spectrum has been broadened using a Lorentzian of 1 meV FWHM. Here transitions of the type $WL_h\rightarrow$electron-$L_zL_{xy}$ and hole-$L_zL_{xy}$ →$WL_e$ are highlighted in green (light grey) and blue (dark grey), respectively.

We first look at the manifestation in interband absorption of the electron states that are above the matrix CBM. A subspectrum of the InAs/GaAs QD without WL is highlighted by the red (dark grey) area in Fig. 15. It consists of final electron states that are *not* dot-confined. The initial hole states, in turn, were allowed to be of any type. As a consequence, it is expected that its onset is at $E_c^{\rm mat}-E(S_h)$, corresponding to the transition from $h_0$ to the first $e$-$D_zD_{xy}$ state. This value is marked by a dotted vertical line in Fig. 15. However, we find that the actual onset is above $E_c^{\rm mat}-E(S_h)$. The few peaks in this subspectrum, at ~1.4–1.5 eV and labeled as LL→SILS, correspond to transitions from $h$-$L_zL_{xy}$ states into SILS of the type $L_zL_{xy}$, indicating that, in the absence of a WL, no crossed transitions $h\rightarrow e$-$D_zD_{xy}$ are present. The decomposition also reveals that, in the high energy part, above $E_c^{\rm mat}-E_v^{\rm mat}$, the interband absorption is exclusively due to direct continuum-to-continuum transitions, of type 3 in Fig. 2. We will show below that, even including a WL, the only strong crossed transitions into 2D/3D *electron* final states correspond to SILS or VBS.

For the same system, InAs/GaAs QD without WL, Fig. 15, we see another series of relatively sharp high intensity peaks highlighted in orange (light grey) and labeled as DL →LL. They are overlapped with the direct $h\rightarrow e$ (intradot) peaks, are characterized by an onset at ≃1.15 eV, and extend high in energy, close to the continuum threshold $E_{\rm gap}$. The final (electron) states of these transitions are of type $L_zL_{xy}$, whereas the initial (hole) states are of the type $D_zL_{xy}$ discussed in Sec. IV. These $D_zL_{xy}$ states, with prototypes depicted in Fig. 5, are only laterally ($xy$) dot confined, and appear because of the strain-induced opening and smoothening of the hole confinement. We show in the following that these states have a major role in enabling strong $WL_h\rightarrow e$ transitions.

### A. Wetting layer hole to bound electron crossed transitions $WL_h\rightarrow e$ are strong

As expected, when a 4 ML thick WL is included in the structure (corresponding spectrum shown in Fig. 16), the most obvious change can be observed in the energy range ~1.2,…,1.5 eV of the interband absorption. This corresponds to $E_c^{\rm WL}-E_v^{\rm WL}$, where $E_c^{\rm WL}$ ($E_v^{\rm WL}$) are the first unbound

electron (hole) solutions of Eq. (2) in the presence of the WL. We have marked this value in Fig. 16 by a dashed line. Consequently, *direct* $WL_h \rightarrow WL_e$ transitions (of type 2 in Fig. 2) occur only right of the $E_c^{WL}-E_v^{WL}$ threshold. For the particular thickness of 4 ML corresponding to the calculations illustrated in Fig. 16 $E_c^{WL}-E_v^{WL}=1.21$ eV, whereas it has been obtained as 1.33 and 1.43 eV for thicknesses of 3 and 2 MLs, respectively.

We have separated out of the full absorption spectrum of Fig. 16 the crossed transitions of type $WL_h \rightarrow e\text{-}L_zL_{xy}$, i.e., those labeled type 5 in Fig. 2. These are outlined by green (light grey) areas in Fig. 16. With an onset at $\simeq 1.12$ eV, they are obviously well below the WL onset $E_c^{WL}-E_v^{WL}$, and in excellent qualitative agreement with the experimental and theoretical results.[23,25] Most significantly, the pronounced peaks (at 1.13, 1.21, 1.27, and 1.33 eV) that can be seen in this subspectrum originate from *hybrid* $(h\text{-}D_zL_{xy})\text{-}WL_h$ states, and not from $WL_h$.[23] This is suggested by the similar pattern of these peaks with that of the system without WL, Fig. 15. Indeed, since nothing prevents WL states to penetrate the dot, such WL-dot hybridization can easily occur. To conclude, we have found $WL_h \rightarrow e$ crossed transitions to be allowed but this only happens because the $h\text{-}D_zL_{xy}$ states illustrated in Fig. 5 mediate an efficient dot-WL hybridization.

### B. Bound hole to wetting layer electron crossed transitions $h \rightarrow WL_e$ are weak

The results presented in Fig. 15 for the InAs/GaAs QD without WL have shown that "crossed" transitions of the type $h\text{-}L_zL_{xy} \rightarrow e\text{-}D_zD_{xy}$ are weak. We could see only a few peaks due to electron SILSs. In a similar manner as we did above for the $WL_h \rightarrow e\text{-}L_zL_{xy}$ transitions, we separate the subspectrum of type $h\text{-}L_zL_{xy} \rightarrow WL_e$ (transitions of type 6 in Fig. 2) for the InAs/GaAs QD with a 4 ML thick WL. This subspectrum is shown in Fig. 16 by highlighted blue (dark grey) areas. The onset of this spectrum nearly coincides with the WL onset $E_c^{WL}-E_v^{WL}$. Moreover, apart from a few peaks, we see that the $h\text{-}L_zL_{xy} \rightarrow WL_e$ crossed transitions appear much weaker than the corresponding $WL_h \rightarrow e$ ones [shown in green (light gray)]. This corresponds to the expectations formulated when discussing intraband absorption for the same system, in Sec. V B. *We find that* $WL_e$ *states are repelled* by the QD in realistic strained structures. In addition, similarly to the intraband absorption, we observe a twofold manifestation of the strain-induced wings in the electron confining potential: (i) by preventing the WL states to hybridize with the dot states, the potential wings play the central role in impeding any strong $h\text{-}L_zL_{xy} \rightarrow WL_e$ crossed transition; (ii) several sharp transitions are possible to appear as a result of the presence of SILS.

## VII. CONCLUSIONS

Using a multiband atomistic pseudopotential approach we investigated the nature of hole and electron states in self-assembled quantum dots (QDs). We have shown that, because of the nonhomogeneous strain present at the dot-matrix interface, the confining potential, for both holes and electrons, is strongly distorted. These effects were analyzed by comparing results obtained for the strain-free InAs/GaSb QDs to those obtained for the strained InAs/GaAs QDs. We suggest a realistic interpretation of interband and intraband absorptions in self-assembled QDs based on our results. The main conclusions we arrived at can be summarized as follows:

(i) The electron confining potential exhibits wings in the vicinity of the dot, wings that create a local barrier for the electron states. As a consequence, strain-induced localized states (SILSs), energetically located within the matrix/WL continuum were found. These states have pronounced signatures in both interband and intraband absorptions, in the form of sharp, well-defined peaks. Being efficiently shielded by the wings, the SILSs are only weakly coupled to the continuum.

(ii) The comparison of unstrained InAs/GaSb system, exhibiting no such wings, with the strained InAs/GaAs, where the wings are present, revealed that the wings-created local barrier also impedes the electron states dot-WL hybridization. For this reason, crossed transitions of the type bound hole-to-WL electron and bound electron-to-WL electron are practically dark.

(iii) The hole confining potential is wider and smoother than in the simpler steplike model resulting from the unstrained band offset. This leads to the appearance of a new kind of hole states, $h\text{-}D_zL_{xy}$, in-plane localized inside the dot but having tails in the growth direction. Their presence is a manifestation of the dot, not of the WL. Transitions from these states into electron dot-confined states are strong, and energetically located in the region between the intradot and continuum-to-continuum transitions; in fact, where $WL_h \rightarrow e$ would be expected to show up if a WL was present. When a WL is physically present, the $h\text{-}D_zL_{xy}$ states hybridize efficiently with the $WL_h$ states. As a result, strong crossed transitions of the type $WL_h \rightarrow$(bound-electron) are favored.

## ACKNOWLEDGMENTS

This work was funded by the U. S. Department of Energy, Office of Basic Energy Science, Materials Science and Engineering Division under Contract No. DE-AC36-08GO28308 to NREL. G.B. would like to thank Robson Ferreira for fruitful discussions on the literature of virtual bound states. We also acknowledge Vladan Mlinar for discussions on interdiffusion and providing the In/Ga diffusion profiles.

*Corresponding author; alex.zunger@nrel.gov

[1] U. Woggon, *Optical Properties of Semiconductor Quantum Dots*, Springer Tracts in Modern Physics (Springer Verlag, Berlin, 1997).
[2] L. Jacak, P. Hawrylak, and A. Wójs, *Quantum Dots* (Springer Verlag, Berlin, 1998).
[3] D. Bimberg, M. Grundmann, and N. N. Ledentsov, *Quantum Dot Heterostructures* (Wiley, New York, 1999).
[4] V. A. Shchukin, N. N. Ledentsov, and D. Bimberg, *Epitaxy of Nanostructures, Nanoscience and Technology* (Springer Verlag, Berlin, 2004).
[5] I. Kegel, T. H. Metzger, P. Fratzl, J. Peisl, A. Lorke, J. M. Garcia, and P. M. Petroff, Europhys. Lett. **45**, 222 (1999).
[6] J. Stangl, V. Holý, and G. Bauer, Rev. Mod. Phys. **76**, 725 (2004).
[7] E. Dekel, D. Gershoni, E. Ehrenfreund, D. Spektor, J. M. Garcia, and P. M. Petroff, Phys. Rev. Lett. **80**, 4991 (1998).
[8] M. Baier, F. Findeis, A. Zrenner, M. Bichler, and G. Abstreiter, Phys. Rev. B **64**, 195326 (2001).
[9] M. Ediger, G. Bester, A. Badolato, P. M. Petroff, K. Karrai, A. Zunger, and R. J. Warburton, Nat. Phys. **3**, 774 (2007).
[10] R. Ferreira and G. Bastard, Nanoscale Res. Lett. **1**, 120 (2006).
[11] P. Lelong, S. W. Lee, K. Hirakawa, and H. Sakaki, Physica E (Amsterdam) **7**, 174 (2000).
[12] D. P. Nguyen, N. Regnault, R. Ferreira, and G. Bastard, Phys. Rev. B **71**, 245329 (2005).
[13] C. Kammerer, G. Cassabois, C. Voisin, C. Delalande, P. Roussignol, and J. M. Gérard, Phys. Rev. Lett. **87**, 207401 (2001).
[14] Y. Toda, O. Moriwaki, M. Nishioka, and Y. Arakawa, Phys. Rev. Lett. **82**, 4114 (1999).
[15] G. Bastard, U. O. Ziemelis, C. Delalande, M. Voos, A. C. Gossard, and W. Wiegmann, Solid State Commun. **49**, 671 (1984).
[16] A. Messiah, *Quantum Mechanics* (Dover, Mineola, NY, 1999).
[17] V. Popescu, G. Bester, and A. Zunger, Appl. Phys. Lett. **95**, 023108 (2009).
[18] A. Luque and A. Martí, Phys. Rev. Lett. **78**, 5014 (1997).
[19] J. Phillips, K. Kamath, and P. Bhattacharya, Appl. Phys. Lett. **72**, 2020 (1998).
[20] S. Maimon, E. Finkman, G. Bahir, S. E. Schacham, J. M. Garcia, and P. M. Petroff, Appl. Phys. Lett. **73**, 2003 (1998).
[21] D. Pan, E. Towe, and S. Kennerly, Appl. Phys. Lett. **73**, 1937 (1998).
[22] C. Kammerer, C. Voisin, G. Cassabois, C. Delalande, P. Roussignol, F. Klopf, J. P. Reithmaier, A. Forchel, and J. M. Gérard, Phys. Rev. B **66**, 041306(R) (2002).
[23] A. Vasanelli, R. Ferreira, and G. Bastard, Phys. Rev. Lett. **89**, 216804 (2002).
[24] H. Htoon, D. Kulik, O. Baklenov, A. L. Holmes, T. Takagahara, and C. K. Shih, Phys. Rev. B **63**, 241303(R) (2001).
[25] R. Oulton, J. J. Finley, A. I. Tartakovskii, D. J. Mowbray, M. S. Skolnick, M. Hopkinson, A. Vasanelli, R. Ferreira, and G. Bastard, Phys. Rev. B **68**, 235301 (2003).
[26] Y. I. Mazur, B. L. Liang, Z. M. Wang, G. G. Tarasov, D. Guzun, and G. J. Salamo, J. Appl. Phys. **101**, 014301 (2007).
[27] A. J. Williamson, L. W. Wang, and A. Zunger, Phys. Rev. B **62**, 12963 (2000).
[28] A. Zunger, Phys. Status Solidi B **224**, 727 (2001).
[29] L. He, G. Bester, and A. Zunger, Phys. Rev. B **70**, 235316 (2004).
[30] G. A. Narvaez, G. Bester, and A. Zunger, J. Appl. Phys. **98**, 043708 (2005).
[31] K. Kim, P. R. C. Kent, A. Zunger, and C. B. Geller, Phys. Rev. B **66**, 045208 (2002).
[32] P. N. Keating, Phys. Rev. **145**, 637 (1966).
[33] R. M. Martin, Phys. Rev. B **1**, 4005 (1970).
[34] R. Magri and A. Zunger, Phys. Rev. B **65**, 165302 (2002).
[35] *Semiconductors: Group IV and III-V Compounds*, Landolt-Börnstein, New Series, Group III, Vol. 17, edited by O. Madelung (Springer, Berlin, 1982).
[36] *Semiconductors: Intrinsic Properties of Group IV Elements and III-V, II-VI, and I-VII Compounds*, Landolt-Börnstein, New Series, Group III, Vol. 22, edited by O. Madelung (Springer, Berlin, 1987).
[37] I. Vurgaftman, J. R. Meyer, and L. R. Ram-Mohan, J. Appl. Phys. **89**, 5815 (2001).
[38] L.-W. Wang and A. Zunger, Phys. Rev. B **59**, 15806 (1999).
[39] V. Popescu, G. Bester, M. C. Hanna, A. G. Norman, and A. Zunger, Phys. Rev. B **78**, 205321 (2008).
[40] A. J. Williamson and A. Zunger, Phys. Rev. B **59**, 15819 (1999).
[41] G. E. Pikus and G. L. Bir, Sov. Phys. Solid State **1**, 1502 (1959).
[42] G. E. Pikus and G. L. Bir, Phys. Rev. Lett. **6**, 103 (1961).
[43] J. D. Eshelby, J. Appl. Phys. **25**, 255 (1954).
[44] A. J. Williamson and A. Zunger, Phys. Rev. B **58**, 6724 (1998).
[45] R. Buczko and F. Bassani, Phys. Rev. B **54**, 2667 (1996).
[46] E. A. Zibik, W. H. Ng, L. R. Wilson, M. S. Skolnick, J. W. Cockburn, M. Gutierrez, M. J. Steer, and M. Hopkinson, Appl. Phys. Lett. **90**, 163107 (2007).
[47] R. Seguin, A. Schliwa, T. D. Germann, S. Rodt, K. Pötschke, A. Strittmatter, U. W. Pohl, D. Bimberg, M. Winkelnkemper, T. Hammerschmidt, and P. Kratzer, Appl. Phys. Lett. **89**, 263109 (2006).
[48] A. Schliwa, M. Winkelnkemper, and D. Bimberg, Phys. Rev. B **76**, 205324 (2007).
[49] V. Mlinar, A. Schliwa, D. Bimberg, and F. M. Peeters, Phys. Rev. B **75**, 205308 (2007).
[50] H. S. Carslaw and J. C. Jaeger, *Conduction of Heat in Solids* (Oxford University Press, New York, 1986).
[51] P. Piquini, A. Zunger, and R. Magri, Phys. Rev. B **77**, 115314 (2008).
[52] A. Vasanelli, M. De Giorgi, R. Ferreira, R. Cingolani, and G. Bastard, Physica E (Amsterdam) **11**, 41 (2001).